



# The Effect of Various Wedge Flap Configurations on the Performance of Wind Turbine Airfoil

Asmail A. M. Abdalkarem<sup>1</sup> · Ahmad Fazlizan<sup>1</sup> · Wan Khairul Muzammil<sup>2</sup> · Chin Haw Lim<sup>1</sup> · Adnan Ibrahim<sup>1</sup> · Kok Hoe Wong<sup>3</sup> · Hussein A. Kazem<sup>4</sup>

Received: 7 August 2023 / Accepted: 9 December 2023  
© The Author(s), under exclusive license to Shiraz University 2024

## Abstract

Controlling turbulent flow to improve wind turbine airfoils' aerodynamic characteristics is a desirable task. The current study evaluated the potential of adding a wedge flap (WF) at the trailing edge of the NACA0021 airfoil. The effect of different WF heights and lengths on optimum height ( $L/H$ ) on the aerodynamic performance and flow over the airfoil has been studied numerically using two-dimensional computational fluid dynamics simulation. The simulation solves the Reynolds-Averaged-Navier–Stokes with shear stress transport  $k-\omega$  turbulent model. The results indicate that adding WF can effectively suppress flow separation and improve aerodynamic efficiency in all studied cases compared to clean airfoil. The aerodynamic performance is influenced significantly by the height of WF compared to the slight influence by the length at  $L/H < 1$ . Inclined WF achieves the highest lift and lift-to-drag values with total maximum increments of 71.67% and 45.79%, respectively, at optimum height and length with 6% $c$  and 1% $c$ , respectively, in comparison with the clean airfoil case. The results observed that WFs have advantages over the Gurney flaps discussed in this study. WF appears to be an effective passive flow control device that can be used in wind turbines if its dimensions are properly chosen.

**Keywords** CFD · NACA0021 · Wind turbine · Wedge flap · Passive flow control

## 1 Introduction

Harvesting energy from the wind is considered one of the most viable sources of clean energy (Ramlee et al. 2020). Wind turbines are classified into vertical axis wind turbines (VAWTs) and horizontal axis wind turbines (HAWTs). Although HAWT has higher efficiency and its technology is better developed due to the benefits from the enormous investment in the last decades to overcome many deficiencies (Akhlagi et al. 2023; Paraschivoiu 2002). In contrast, there are still existing various challenges with HAWTs

currently, such as noise pollution, ecological problems, and fatigue issues (Ni et al. 2021). Compared with HAWTs, VAWTs have been gaining increasing attention for several advantages, i.e., ability to withstand high turbulence and better performance in complex urban areas, omni-directional without yawing mechanism, lower cost (manufacturing, installation and maintenance) and it is designed for low wind speed. Despite the practical advantages of the VAWT, the VAWTs face some disadvantages: low power generation due to dynamic stall and blade wake interactions and difficulty to self-start (Farajyar et al. 2023; Li et al. 2017; Paraschivoiu 2002).

The phenomenon of dynamic stall refers to the boundary layer separation that occurs to the unsteady flow over aerodynamic bodies. This phenomenon appears with various current applications in aeronautics, hydrodynamics, and wind engineering, mainly on the wings and rotating rotor blades, including VAWTs. Dynamic stall occurs when VAWT blades operate in a wide range of angle of attack (AOA) periodically at different azimuth angles at low values of the tip speed ratio (TSR) of less than 4 (Asadbeigi et al. 2023). It generally depends on the airfoil configuration, Reynolds

✉ Ahmad Fazlizan  
a.fazlizan@ukm.edu.my

<sup>1</sup> Solar Energy Research Institute (SERI), University Kebangsaan Malaysia, 43600 Bangi, Selangor, Malaysia

<sup>2</sup> Energy Research Unit, Faculty of Engineering, University Malaysia Sabah, Jln. UMS, 88400 Kota Kinabalu, Malaysia

<sup>3</sup> Carbon Neutrality Research Group (CNRG), University of Southampton Malaysia, 79200 Iskandar Puteri, Malaysia

<sup>4</sup> Faculty of Engineering, Sohar University, PO Box 44, PCI 311 Sohar, Oman

number (Re), number of blades, chord length and TSR (Hand et al. 2017; Jha et al. 2020). It significantly impacts noise levels, vibration, and power extraction. Hence, VAWT urgently requires effective and low-cost devices to increase efficiency.

Many effective techniques have been proposed for suppressing dynamic stalls and enhancing the power coefficient of turbomachinery, including the VAWT. These techniques can be divided based on active and passive flow control techniques. Active flow control methods can suppress the dynamic stall by adjusting the control parameters. However, these techniques required complex control mechanisms, algorithms, maintenance, weight, and additional energy expenditure during operation for flow structure improvements, which any benefits must outweigh (Azlan et al. 2023). By contrast, passive flow control techniques, e.g.,, cited by Zhu et al. (2018), including; leading-edge micro cylinder, slots, Gurney flaps (GFs), thin plates at trailing edge, passive movable flaps, leading edge serrations, tilted blades, J-shaped airfoil, airfoil with a cavity, variable droop leading-edge, adaptive blades, leading edge slat, non-circular gap, flow-deflecting airfoil and vortex generators, are usually cheap, easier to implement, and no additional energy needed. The effect of dimples (Azlan et al. 2023), surface roughness (Özkan and Erkan 2022) and slots (Belamadi et al. 2022) on the blades are some of the recent investigations on passive flow-field control for performance enhancement of HAWT. GF, micro tab, vortex generator, and leading-edge slat are the most common passive flow control technology widely used in straight-bladed VAWTs (Zhong et al. 2019).

The Gurney flap is a small plate added to the airfoil's trailing edge (TE) perpendicular to the chord line. It was first proved by Liebeck (1978) after its invention by Dan Gurney in the 1970s. Liebeck found that adding GF to the symmetrical airfoil known as a Newman airfoil increased the lift at different AOAs with a penalty in drag with an optimum GF height of 1.25% of the chord length ( $c$ ). He also concluded that the GF height should have remained between 1 and 2%  $c$  and kept submerged within the local boundary layer to avoid rapid increment in drag to obtain a beneficial L/D ratio, which is supported by the results of Myose et al. (1996), Giguère et al. (1997) and Li et al. (2002). Liebeck also proposed that the adding GF changed the flow structure around the TE. Since then, and with the development of computational fluid dynamics (CFD), many geometrical modifications of the GF to enhance the lift have been proposed by researchers covering several applications, such as VAWTs.

Many flow control techniques have been proposed to enhance lift to obtain a high lift-to-drag ratio; however, the drag is also increased due to downstream flow separation. The attempts to propose, study, or investigate the drag reduction devices in the literature are limited to some

works (Bechert et al. 2000). Studied different GF modifications, including GF with slite and GF with holes and later by Meyer et al. (2006) and Lee (2009); the aim of these modifications is to stabilize the wake flow behind the TE by generating jet flows disrupted the periodic wake behind the flap thus, control the size and location of a von Karman vortex street to reduce the flow unsteadiness, which results in a drag reduction. Compared to solid flap, the magnitude of lift and drag coefficients decreased; however, the decrease in drag outweighed the lift loss, resulting in an improving lift-to-drag ratio.

A wedge flap (WF) that can reduce drag can act as a passive control device placed at or near the TE of the wings and rotor blades. It helps to improve the lift coefficient, reduce the drag coefficient, and improve the overall performance of an airfoil compared to the GF. The WF and the divergent trailing edge (DTE) are similar TE devices designed to increase airfoil efficiency at cruise conditions (Storms and Jang 1994). Only a few studies are concerned with deploying WFs, GF filled-in, and DTEs as flow control devices in literature, as shown in Table 1. To conclude, the working principles of DTEs and WFs are quite similar to the GFs.

Although the literatures listed in Table 1 showed that the WF has initial promises resulted in power output exceeding GFs if properly chosen its dimensions, since it can control its lift and drag by adjusting its height and length. There are shortcomings in the study of the WF as flow control device such as most of the previous studies conducted airfoils equipped with WFs or DTEs in aircraft operation conditions and may not be viable for other applications such as VAWTs. Even in other fields, past researchers that studied WFs limited to studying few numbers of heights and their differential. However, they did not study the effect of heights in a systematic manner, for example starting from the lowest height to the maximum possible height can achieve the best performance. In addition to height, WF effectiveness influences by length, most of previous research limited to the performance at fixed length and this dimension can be studied systematically at various lengths to determine its effect on performance and its relationship to height to obtain the best length at a certain height ( $L/H$ ). Furthermore, previous studies were poor in presenting a comparison of the performance of the GF Vs WF over a wide range of AOAs..

Generally, the use of different airfoil profile can change the power and momentum outputs. Symmetrical airfoils are well-known for their effectiveness with VAWTs, among them NACA0021 which is has a relatively large thickness. It is widely used for VAWT application with reasonable performance (Balduzzi et al. 2021; Du et al. 2019; Holst et al. 2019b; Mohamed 2012). However, previous studies were limited to employing asymmetrical airfoils with WF. Moreover, there is also a lack in studying the effect of the

**Table 1** Summary of wedge flaps, divergent trailing edges and filled-in Gurney flaps that have been attached to the airfoil

Author/year	TE modification	Problem/objective	Geometrical parameters			Operational parameters	Methodology	Main finding
			Airfoil details	TE Height	TE length/angle			
Boyd (1985)	Wedge flap	Studied the effect of WF attached to the trailing edge of the airfoil on the aerodynamic performance	Airfoil type: Transonic airfoil	0.5–1.5% <i>c</i>	Angle = 15°–45°	$M = 0.82\text{--}0.84$ $\alpha = 0^\circ\text{--}8^\circ$	Experimentally in wind tunnel	Invented wedge could improve the $C_L$ and reduces the $C_D$ , providing an overall increase in fuel economy at cruise conditions at a wedge angle between 15° and 45°, height is 0.5% <i>c</i> and preferred placed at 0–1% <i>c</i> from TE
Neuhart and Pendergraft (1988)	Gurney flap filled-in	Investigated the effect of the airfoil TE equipped with various flaps named: GF, serrated GF, and filled-in GF on the flow separation on a wing upper surface	Airfoil type: NACA0012 $c = 0.114$ m AR = 6.7 Span = 0.381 m	4.2% <i>c</i>	$L = 10\%c$	$U_\infty = 0.076$ m/s AOA = 0°–5° Re = 8588	Experimentally in water tunnel by visual observations of the flow field	At AOA = 3.5° GF delayed the separation slightly more than filled-in GF, which could lead to a decrease in filled-in GF performance
Bloy et al. (1997)	Wedge flap	Tested and compared $C_L/C_D$ for five flap shapes with the same length named: 45° WF, 45° flap, 90° WF, 90° GF and square section	Airfoil type: NACA5414 $c = 0.152$ m Span = 0.762 m	2% <i>c</i>	$L = 2\%c$	$U_\infty = 52$ m/s AOA = -5°–20° Re = $5.7 \times 10^5$ TI = 0.6%	Experimentally in wind tunnel	Rearward inclined flaps could improve performance more efficiently than other tested flaps. The 45-deg WF produced the highest $C_L/C_D$ ratio throughout all studied flaps

Table 1 (continued)

Author/year	TE modification	Problem/objective	Geometrical parameters			Operational parameters	Methodology	Main finding
			Airfoil details	TE Height	TE length/angle			
Bechert et al. (2000)	Divergent trailing edge	Studied the effect of various GF modifications (e.g., serrated, slits, holes and DTEs) in drag reduction compared to normal GF	Airfoil type: HQ17 $c=0.5\text{ m}$	1% 1% 1% 1%	$L=2.3\%$	$M=0.1$ $AOA=-10^\circ$ to $15^\circ$ $Re=5 \times 10^5$ $Re=1 \times 10^6$	Experimentally in wind tunnel	In DTE case, the $C_D$ considerably decreased, and $C_L$ decreased compared to GF with the same height. A bigger DTE produced aerodynamic effect comparable to a smaller GF effect which provides a greater mechanical stiffness and stability of the wing
Richter and Rosemann (2002)	Divergent trailing edge	Investigated the influence of GFs versus DTEs on the airfoil's performance at transonic speeds	Airfoil type: Transonic airfoil VC-Opt $c=0.4\text{ m}$ span = 1 m $t/c=0.0818$	0.5%, 1%, 1% 1% 1%	$L=2\%$	$M=0.755, 0.775$ and $0.790$ $AOA=-3^\circ$ to $5^\circ$ $Re=5 \times 10^6$	Experimentally in transonic wind tunnel	Increases in $C_L$ and $C_D$ produced by GF attributed to the largest additional circulation due to adding GF. While the DTE shows smaller increase of circulation due to smoother flow deflection leading to slightly less lift but considerably less drag with enhancing $L/D$ ratio
Timmer and Van Rooij (2003)	Wedge flap	Investigated the effects of adding various aerodynamic devices such as GFs and WFs on the aerodynamic performance of DUT	Airfoil type: DU 93-W-210 $c=0.6\text{ m}$ $t/c=0.21$	1% 1% 1%	$L=1\%$ , $2\%$ , $4\%$	$U_\infty=42\text{ m/s}$ $AOA=0^\circ-20^\circ$ $Re=2 \times 10^6$	Experimentally in wind tunnel	WFs and GF show similar TE devices characteristics at 1% height, while with increasing of upstream wedge length the maximum $C_L$ and $C_D$ reduced

Table 1 (continued)

Author/year	TE modification	Problem/objective	Geometrical parameters			Operational parameters	Methodology	Main finding
			Airfoil details	TE Height	TE length/angle			
Troolin et al. (2006)	Filled-in Gurney flap	Studied the flow structure around standard GFs versus GF filled in	Airfoil type: NACA0015 $c=0.1905$ m Span = 0.3048 m AR = 1.6	4% $c$	$L = 30\%c$	$U_{\infty} = 15.4$ m/s AOA = $0^{\circ}$ – $10^{\circ}$ Re = $2 \times 10^5$	Experimentally in wind tunnel	A major part of the lift increment produced by the GF results from the upstream shedding and its effect on the trailing wake
Mohammadi et al. (2012)	Wedge flap	Studied the aerodynamic performance of DU 91-W2-250 airfoil equipped with TE wedge, TE curved wedge flap and GF	Airfoil type: DU 91-W2-250 $c = 1$ m $t/c = 0.25$	1% $c$ , 2% $c$	$L = 1.5\%c$ , 2.1% $c$ , 3% $c$	AOA = $0^{\circ}$ – $10^{\circ}$ Re = $2 \times 10^6$	CFD simulation using SST-Transitional turbulence model	Both types of WFs have $C_L/C_D$ exceeded the GF with the same height of 1% $c$ . In both WFs $C_D$ decreased compared to GF which is attributed to disappears of separation bubbles at the upstream of the TE

inclined WFs on the performance of the airfoil and most of past researches limited to perpendicular ones.

This paper aims to study the effects of NACA0021 airfoil equipped with WF on the aerodynamic performance and the flows over the mid-span section of airfoil blade using ANSYS FLUENT code to solve the steady Reynolds-Averaged Navier–Stokes equation (RANS) at a wide range of AOAs. The novelty of this paper will include:

- Studying the impact of various heights of the WF added to the symmetrical airfoil NACA0021 on the airfoil's aerodynamic performance, aiming to determine systematically the optimal height at highest lift-to-drag ratio can be achieved.
- In addition to height, the current paper will investigate systematically the effect of changing the length of WF at optimal height, aiming to obtain the best length- to-height ratio that maximizes performance.
- The influence of the wedge angle for different cases will be studied to identify the optimal wedge angle can achieve the highest performance.
- A comparison between present results of studying WF performance and the results of the GF performance from literature under the same conditions will be presented and discussed in this paper.
- The effect of the flow on the trailing edge of the airfoil including streamlines, velocity profiles, and pressure contours will be studied to gain a deeper understanding of the flow behavior on an airfoil with an added WF at various AOAs, illustrating the positive impact of the WF in delaying separation point compared to the airfoil without WF.

The paper also presents flow visualizations from the simulations, including streamlines, velocity profiles, and pressure contours.

## 2 Methodology

In the current study, the ANSYS FLUENT (Version 2020 R1) solver based on the finite volume method is employed to predict the fluid flow phenomena by numerically solving the governing mathematical equations. The simulations are carried out in a two-dimensional manner to model the mid-span segment of the blade, with the effects of spanwise flow and tip loss are neglected. According to the literature, 2D simulations for this case are able to provide reliable data when compared to measured data, all while maintaining reasonable computational costs (Bangga et al. 2021; Florin et al. 2014; Rezaeiha et al. 2018b). An overview of the sequence steps of CFD Modeling is shown in Fig. 1.

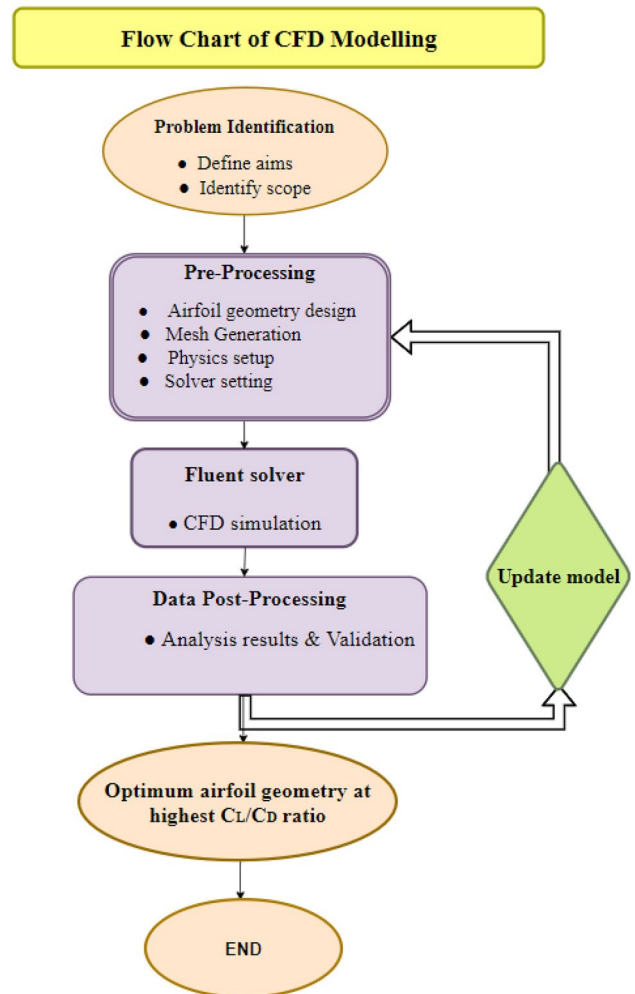


Fig. 1 Flow chart of CFD Modeling

### 2.1 Airfoil Geometry and Test Plane

The symmetric 4-digit NACA series is the most widely used for VAWT applications. It has a relatively large thickness and improves turbine performance. Mohamed (2012) studied the performance H-rotor Darrieus turbine using the symmetric and non-symmetric NACA airfoils through CFD simulation. Its results show that NACA0021 gives the highest performance at low TSR  $< 4$  among the symmetric NACA00xx series. Du et al. (2019) tested experimentally three-bladed H-Darrieus turbine with different airfoil profiles. Their study showed that the NACA0021 profile improves self-starting capability, enhancing power at low TSR. In the present study, 4-digit NACA0021 (Fig. 2) was selected with 140 mm chord length ( $c$ ), which has been studied by some researchers in different works (Holst et al. 2019a; b; Balduzzi et al. 2021).

The effect of different WF dimensions (height and length) and the mounting angles were simulated and compared to



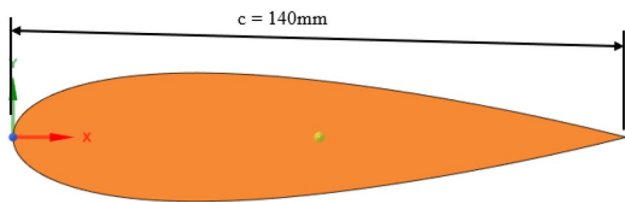


Fig. 2 Airfoil geometry of NACA0021

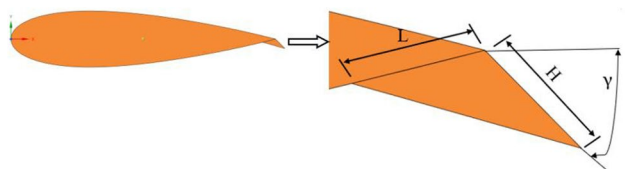


Fig. 3 Geometry of NACA0021 with WF

the clean airfoil. The geometry of the NACA0021 airfoil equipped with WF is shown in Fig. 3, where  $H$  refers to the height of WF perpendicular to the chord line,  $L$  is the length of WF extended upstream on the lower airfoil surface, and  $\gamma$  is the mounting angle between the WF and the chord line of the airfoil. In this case, the dimensions of WF selected to be at the same length  $L=H$  or  $L/H$  ratio = 1.

Various wing flap (WF) heights were studied, and the lift coefficient ( $C_L$ ) and drag coefficient ( $C_D$ ) were assessed to reach the optimal lift-to-drag ratio ( $C_L/C_D$ ). The coefficients acting on the airfoil were calculated using Eqs. 1 and 2. The flap's height ( $H$ ) and length ( $L$ ) were relatively defined to the chord length. Then, the influence of different mounting angles of  $90^\circ$  and  $45^\circ$  has been studied at different heights, reaching the optimum flap angle. Finally, the influence of different  $L/H$  ratios with various mounting angles and optimum fixed heights on the aerodynamic performance of static NACA0021 has been investigated.

$$C_L = \frac{F_L}{0.5\rho S U^2} \tag{1}$$

$$C_D = \frac{F_D}{0.5\rho S U^2} \tag{2}$$

where  $F_L$  and  $F_D$  are the lift and drag forces acting on the blade section,  $\rho$  is the air density,  $S$  is the area, and  $U$  is the air speed.

### 2.2 Governing Equations and Numerical Solutions

The governing equations of CFD are the Reynolds-averaged Navier–Stoke (RANS) equations derived from the conservation law of the physical properties of working fluid: mass,

energy, and momentum. The RANS equations for the two-dimensional steady incompressible flow can be written in a conservative form continuity equation and a momentum equation, as shown below (Anderson et al. 2016; White and Xue 2021):

$$\text{Continuity equation, } \frac{\partial \bar{u}_i}{\partial x_i} = 0 \tag{3}$$

$$\text{Momentum equation, } \rho \frac{\partial \bar{u}_i \bar{u}_j}{\partial x_j} = -\frac{\partial \bar{p}}{\partial x_i} + \frac{\partial}{\partial x_j} \left( \mu \frac{\partial \bar{u}_i}{\partial x_j} - \rho \bar{u}'_i \bar{u}'_j \right) + S_i \tag{4}$$

where the instantaneous value of velocity,  $u$  is expressed by the sum of its mean and the fluctuating part  $\bar{u}_i$  and  $\bar{u}'_i$  of  $i$  direction, respectively, as:  $u = \bar{u}_i + \bar{u}'_i$ ,  $\bar{p}$  is the mean pressure,  $\mu$  is the dynamic viscosity coefficient,  $\rho$  is the density,  $\rho \bar{u}'_i \bar{u}'_j$  is the Reynolds stress, and the generalized source term  $S_i$  is the body force term. The energy equation requires heat transfer or high-speed flows where the velocity exceeds a critical limit, and the flow is assumed to be compressible. For the present case, the Mach number was less than 0.3, and the flow could be considered incompressible with constant viscosity; therefore, the energy equations were not solved.

The proposed SST  $k-\omega$  turbulence model considers the effect of turbulent shear stress transportation and has better computational accuracy in capturing the adverse pressure gradient flows. The SST  $k-\omega$  transport equations are shown below:

$$\frac{\partial}{\partial x_i} (\rho k u_i) = \frac{\partial}{\partial x_j} \left( \Gamma_k \frac{\partial k}{\partial x_j} \right) + G_k - Y_k + S_k \tag{5}$$

and

$$\frac{\partial}{\partial x_j} (\rho \omega u_j) = \frac{\partial}{\partial x_j} \left( \Gamma_\omega \frac{\partial \omega}{\partial x_j} \right) + G_\omega - Y_\omega + S_\omega \tag{6}$$

where  $k$  is the turbulence kinetic energy.  $\omega$  the specific dissipation rate.  $G_k$  is the turbulence kinetic energy (KE) due to mean velocity gradients.  $G_\omega$  is the production of the dissipation rate.  $\Gamma_k$  and  $\Gamma_\omega$  are the effective diffusivity of  $k$  and  $\omega$ , respectively.  $Y_k$  and  $Y_\omega$  are the dissipation of  $k$  and  $\omega$ , respectively, due to turbulence.  $S_k$  and  $S_\omega$  are user-defined source terms.

The previous research (Wang et al. 2010) Investigated the ability of the standard  $k-\omega$  and the SST  $k-\omega$  models to correctly simulate the dynamic stall in VAWTs at the low Reynolds number regime. The results concluded that the SST  $k-\omega$  could predict the experimental data sets with reasonable accuracy and the dynamic stall characteristics well captured. Rezaeiha et al. (2019) compared seven different turbulence models commonly used to optimize the most accurate model for CFD simulations of VAWTs. The

**Table 2** Numerical constants and solution methods

Numerical constants	
Turbulence kinetic energy, $k$	0.8
Specific dissipation rate, $\omega$	0.8
Solution methods	
Pressure–velocity coupling	Coupled
Gradient	Set as Least squares cell-based
Pressure, Momentum, Turbulent kinetic energy ( $k$ ), and Specific dissipation rate ( $\omega$ )	Set as Second-order upwind

extensive analysis concluded that only the SST models, including SST  $k-\omega$ , can exhibit reasonable agreement with all the experimental data and predict the power coefficient more accurately with a wide range of TSR. Daróczy et al. (2015) compared five turbulent models widely used in simulations of VAWTs employing two-dimensional versus different experimental works to identify the most suitable model. The results revealed that the  $k-\omega$  SST model agreed well with the experiments.

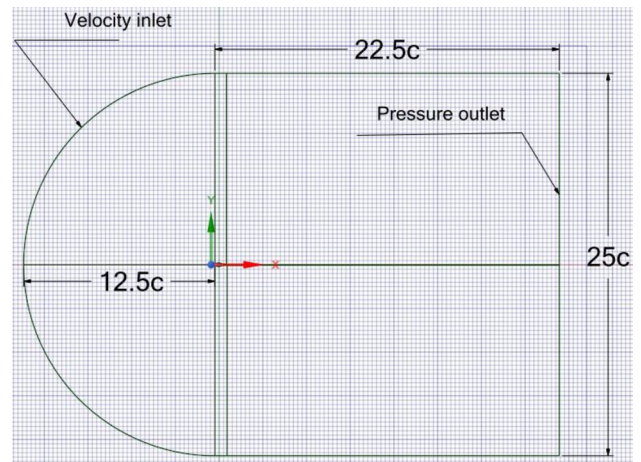
Thus, the turbulence model employed in this study is the shear stress transport (SST)  $k-\omega$ . Also, the transition from laminar to turbulent flow transitional (SST)  $k-\omega$  model was adopted to simulate the flow during and after stall angle at different AOA for accurate results. In this study, numerical simulations were performed using ANSYS FLUENT commercial CFD software. The numerical constants and solution methods in this study are tabulated in Table 2.

### 2.3 Computational Domain and Boundary Conditions

In the simulation of a static aerofoil, the chord length ( $c$ ) is 0.14 m. The Re (Eq. 7) is  $1.8 \times 10^5$ , and the Mach number is 0.06, i.e., thus, the flow is incompressible. The air temperature is 20 °C, while density ( $\rho$ ) and dynamic viscosity ( $\mu$ ) are  $1.204 \text{ kg/m}^3$  and  $1.855 \times 10^{-5} \text{ kg/m s}$ , respectively. Such conditions represent small to medium-scale urban VAWTs (Rezaeiha et al. 2018a).

$$\text{Re} = \frac{c\rho U}{\mu} \quad (7)$$

The computational domain size in the range of 10–20 length /chord has been adopted by many researchers, such as Wang et al. (2017), Yan et al. (2020), Michna et al. (2021). Their results show that this range is sufficient to obtain accurate aerodynamic results. The distance of the inlet and outlet boundaries away from the 1/4 of the airfoil chord length is  $12.5c$  and  $22.5c$ , respectively, and the top and bottom

**Fig. 4** Computational domain dimensions and boundary conditions**Table 3** Boundary conditions for CFD simulations

Boundary	Type
Inlet (Top, Left, Bottom)	Velocity inlet, 20 m/s
Outlet (Right)	Pressure outlet, atmospheric pressure value
Airfoil and the WT surfaces	No-slip wall

boundaries are  $21.75c$  away from the TE. Figure 4 illustrates the computational domain size adopted and the boundary conditions in the present study, while the values are tabulated in Table 3.

### 2.4 Mesh Generation and Dependency Test

Michna et al. (2021) studied extensively different mesh properties and their impacts on the prediction of the accuracy of solutions. Different mesh properties contribute together to improve the mesh quality, increasing the accuracy of calculation results and avoiding the waste of computational time. In the present study, a C-type structured grid was adopted, and the grid distribution near the wall where the boundary layer is located is refined to capture the physics of the flow around the airfoil. Typically, there are 100 layers with a first layer height of 0.016 and a growth rate of 1.097. For the trailing edge, there are 140 layers, and the first layer height and growth rate are 0.015 mm and 1.068, respectively. Figure 5 shows the whole computational domain and a zoomed view of the leading and TEs.

Four types of grids are used in the current simulation to check the dependency of the results on the grids. The details



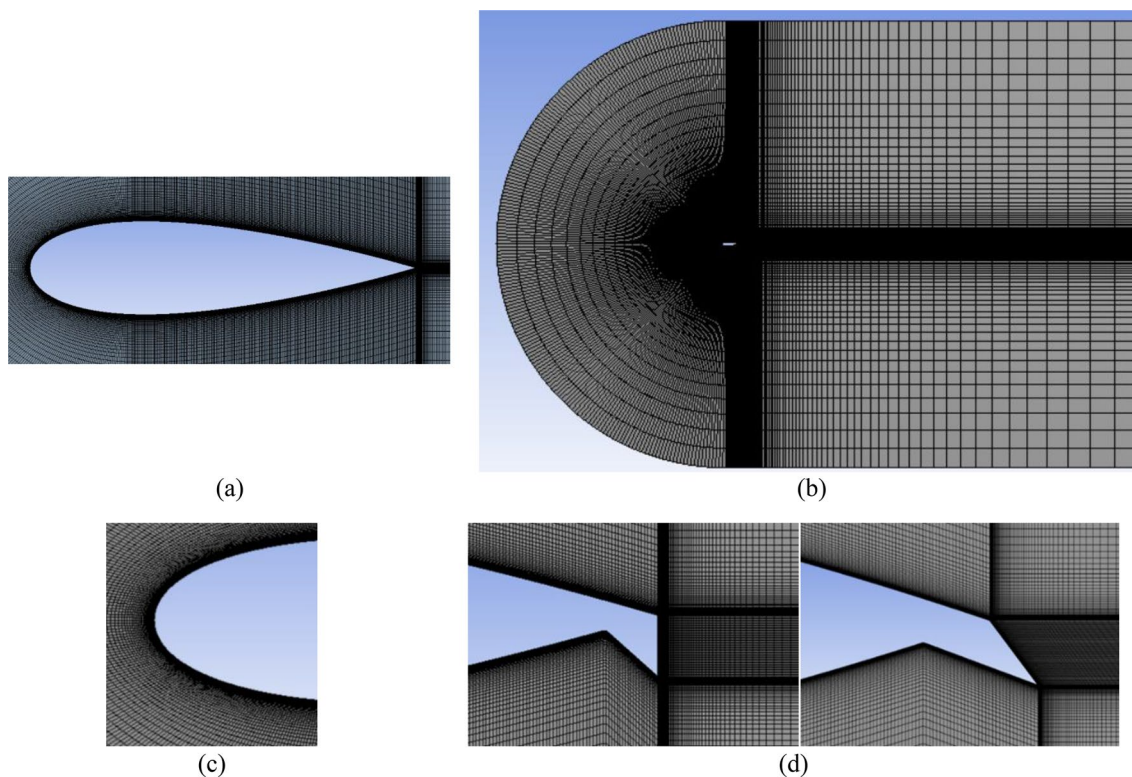


**Fig. 5** Details of the computational grid. **a** Airfoil, **b** C-mesh computational domain (overall mesh), **c** near the leading edge, **d** near the TE around WF

**Table 4** Grid parameters of the clean static NACA0021 airfoil

No	Grid Name	$y^+$	Number of cells
1	G1	$\leq 1$	$2.73 \times 10^4$
2	G2	$\leq 1$	$6.4 \times 10^4$
3	G3	$\leq 1$	$10.8 \times 10^4$
4	G4	$\leq 1$	$13.09 \times 10^4$

of the grids studied at  $Re = 1.8 \times 10^5$  are shown in Table 4. Figure 6 shows the  $C_L$  and lift-to-drag ratio ( $C_L/C_D$ ) variations with a range of AOAs for different grid distributions G1 to G4. The lift coefficient increases with grid refinement from G1 to G3, and G4 shows no more gains in the lift with high mesh density, indicating that the simulation results are independent of the grid numbers selected.

Therefore, the G3 with the number of cells of about  $10.8 \times 10^4$  for the case of clean airfoil was adopted in the present simulation. In contrast, the grid cells for the airfoil equipped with WF are about  $1.16 \times 10^5$ . Figure 6 shows the 800 nodes along the chord line on the upper and lower surfaces of the airfoil mesh with higher concentrations near the leading and TE regions. The non-dimensional distance  $y^+$

value of the first grid point is kept at approximately 1, which means the near-wall mesh is refined enough to resolve the viscous sublayer (Ghazali et al. 2016).

## 3 Results and Discussion

### 3.1 CFD Validation

The present CFD simulation was validated by comparing the aerodynamic characteristics of the static airfoil with measurements from wind tunnel experiments and simulations from the literature. Figure 7 compares experimental data at different turbulence intensity (TI) and computational data for the NACA0021 across a wide range of AOAs at the same conditions, i.e., chord length,  $c = 140$  mm and  $Re = 180K$ . A series of experimental works done by Holst et al. (2019a; b, c), which include the raw and corrected data were used in the validation. According to them, corrections are needed considering the airflow deflection that originated from an open jet and attributed to the lift force generated from the aerodynamic interaction between the flow and the blade surface.

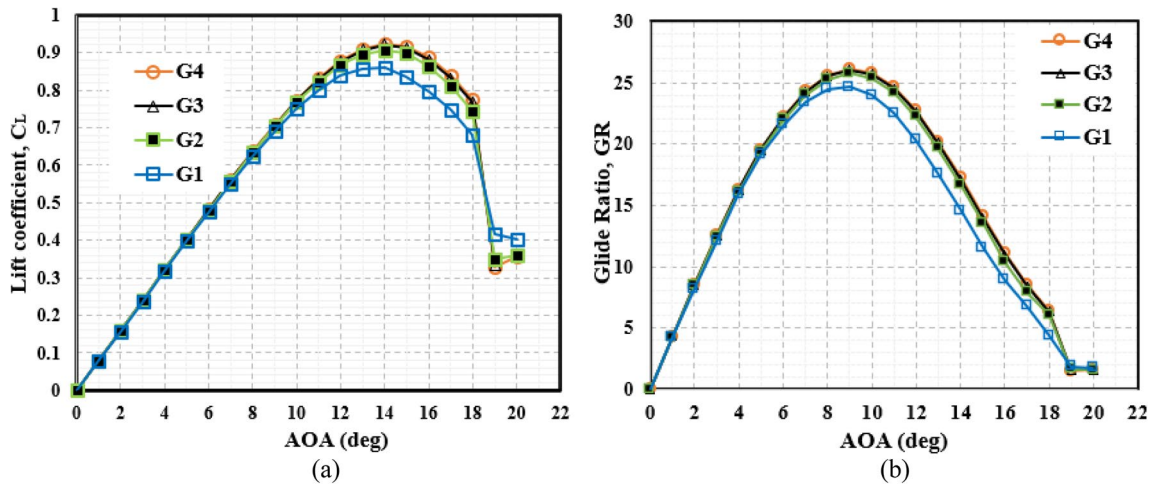


Fig. 6 Comparison of CFD simulation for four grid distributions in the case of a clean static airfoil. **a** Lift, **b** lift-to-drag ratio

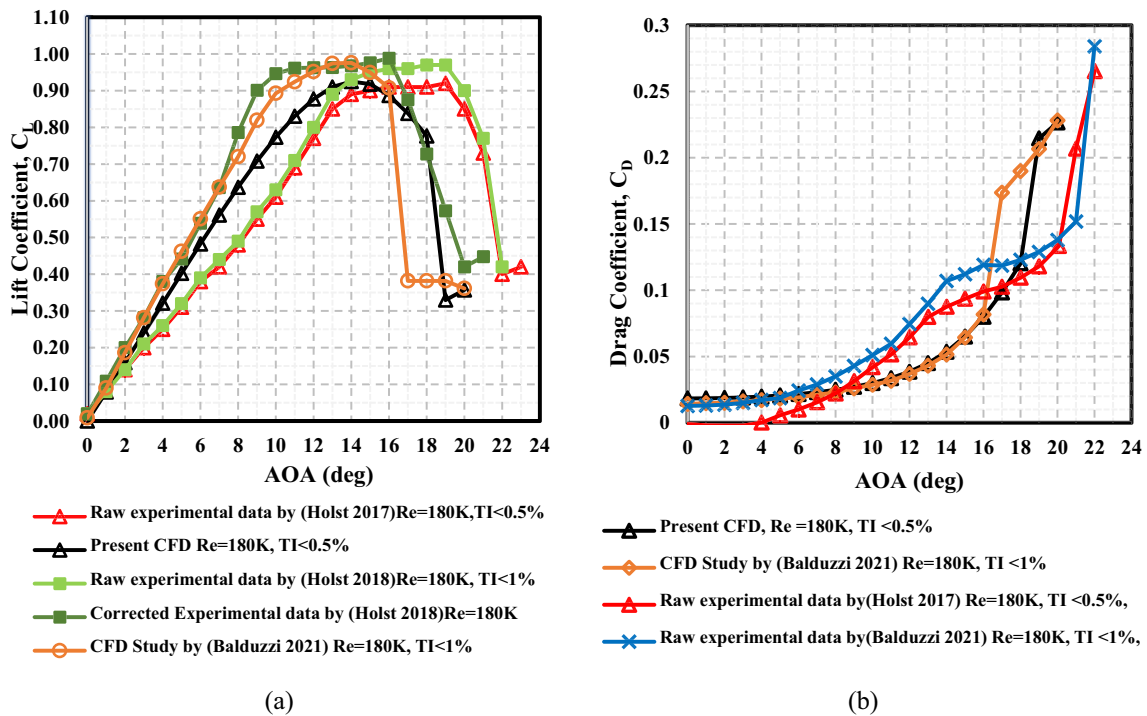


Fig. 7 Validation of static polars (NACA0021 profile) up to stall angle against literature data at  $Re \sim 180K$ . **a** Lift coefficient. **b** Drag coefficient

From the figure, it can be observed that the maximum lift coefficient of uncorrected experimental data by Holst et al. (2019b) with  $TI < 0.5\%$  shows a suitable matching to the present CFD simulation in terms of maximum lift and general behavior. Meanwhile, the corrected experimental data at a  $TI$  of 1% matches well with the simulation by Balduzzi et al. (2021). The typical stall angle of the airfoils occurred when AOA was around 15°. As shown

in Fig. 7, the stall angle of the present CFD simulation occurred at 18°, while for both uncorrected experimental works, the stall occurred at  $AOA = 19^\circ$ . Balduzzi's simulation and corrected experimental work by Holst at  $TI$  less than 1% show the same stall angle at 16°. Balduzzi's CFD work visualizes a nearly constant lift after stalling at AOA between 16° and 20° while the present study and corrected results by Holst show constant lift at AOA

beyond  $19^\circ$  and  $20^\circ$ , respectively. This is caused by a continuous TE stall accompanied with dramatic rises in drag due to separation in the boundary layer.

Figure 7b illustrates a comparison of the drag coefficient with earlier studies. The drag values from our current CFD simulation align well with literature data up to static stalling, with the exception of Holst's work. Holst's drag coefficient values exhibit underestimation in the small AOA range. This discrepancy arises because the computation of drag coefficients relies on the surface pressure distribution, wherein only pressure drag is considered. Contributions from skin friction are inherently absent, influencing the lower AOA region (Holst et al. 2019c).

Hence, the drag coefficient presented by Holst does not include the total drag, especially at low AOAs. In contrast, Balduzzi's simulation and experimental works show consistent behavior with a slight increase in the drag coefficient from the current study at AOAs less than  $6^\circ$ . The general behavior of the lift in the present study shows excellent agreement with the works of literature despite the lack of corrected experimental data by (Holst et al. 2019b).

## 3.2 Effects of the WF Height and Inclination Angle

The effect of the WF height attached to the NACA0021 airfoil and its mounting angle  $\gamma = 90^\circ$  and  $45^\circ$  was investigated. In this section, both WF dimensions  $L$  and  $H$  are considered to have the same length. The effects on aerodynamic characteristics are discussed in the following sections:

### 3.2.1 Effects on Lift Coefficient

Figure 8a, d illustrate the lift coefficient increments with increasing WF heights for  $\gamma = 90^\circ$  and  $45^\circ$ , respectively. Wedge flaps shift the maximum  $C_L$  to the lift side by  $2^\circ$  and  $3^\circ$  for the cases of trailing edge wedge flap with  $\gamma = 90^\circ$  (TEWF-90) and trailing edge wedge flap with  $\gamma = 45^\circ$  (TEWF-45), respectively, in comparison with the clean airfoil case. The increment in maximum values of  $C_L$  with WF height and angle are presented in Table 5. The value of the maximum  $C_L$  increased by 25.09% at 1%c WF height to 70.19% at WF height of 5%c for the TEWF-90 case, while in the case of TEWF-45, the maximum values of  $C_L$  increased from 19.19% at WF with 1%c height to the 69.15% at WF height of 7% of the chord length.

### 3.2.2 Effects on the Drag Coefficient

The  $C_D$  variations with AOA for different TEWF-90 and TEWF-45 heights in comparison with the airfoil baseline case are shown in Fig. 8b, e, respectively. The drag significantly increases as the wedge height increase. Obviously,

as the AOA increases, the  $C_D$  increases as well at the range of AOA between  $0^\circ$  and  $10^\circ$  with a small increase in drag while, the penalty of drag at  $AOA > 10$  increases with the increase of AOA.

### 3.2.3 Effects on Lift-to-Drag Ratio, $C_L/C_D$

Figure 8c, f demonstrate the increases in lift-to-drag ratios with AOAs at different WF heights and with both angles  $90^\circ$  and  $45^\circ$ , respectively, compared with the airfoil without WF. At low to moderate AOAs, the lift increases with the minor penalty of drag, resulting in a significant increase in the lift-to-drag ratio. At moderate to high AOAs, a significant drag penalty decreases the lift-to-drag ratio reaching the stall angle.

- Case of TEWF-90

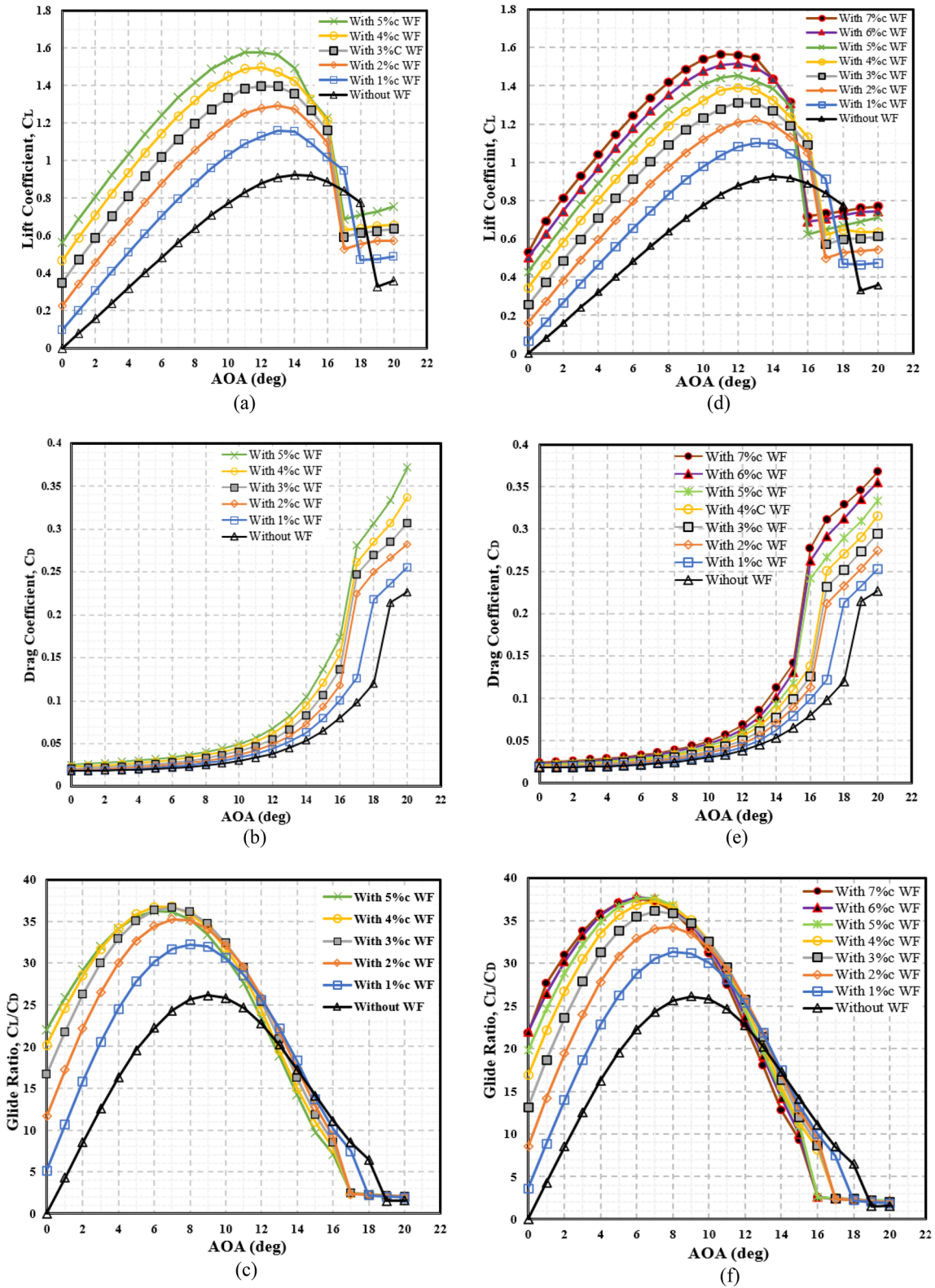
As depicted in Figs. 8c and 9, the maximum lift-to-drag ratio increases with WF heights %1c, %2c, %3c and %4c. In contrast, the maximum lift-to-drag ratio at WF with five height shows a reduction in lift-to-drag ratio due to a significant penalty in drag. This might happen when the WF height exceeds the boundary layer thickness. Therefore, the optimum WF height at a  $90^\circ$  mounting angle is 4%c with a maximum increment in the lift-to-drag ratio of 40.80% at  $AOA = 7^\circ$  compared to the clean airfoil case.

- Case of TEWF-45

Lift-to-drag ratio value increases as illustrated in Figs. 8f and 9 with WF heights of %1c, %2c, %3c, %4c, %5c and 6%c. In contrast, WF with 7%c height shows a reduction in lift-to-drag ratio due to a significant penalty in drag. The optimum WF height at  $45^\circ$  mounting angle is 6%c with a maximum increment in lift-to-drag ratio of 44.57% at  $AOA = 6^\circ$  compared with the clean airfoil case. Therefore, the NACA0021 employed with a WF mounting angle of  $45^\circ$  provides better performance than whose WF is  $90^\circ$ . These results agree with the experimental work by Bloy et al. (1997). From Fig. 9, it can also be concluded that the point of intersection of TEWF-90 and TEWF-45 curves means that the increment of lift-to-drag ratio of 40.7% in comparison with clean airfoil case could be achieved for both cases using WF with the same height at about 3.55% of the chord length.

## 3.3 Effect of the WF Length

The effect of various WF length-to-height ( $L/H$ ) ratios for TEWF-90 and TEWF-45 in comparison with optimum characteristics of WF at heights of 4%c and 6%c, respectively on the aerodynamic performance of the NACA0021 airfoil

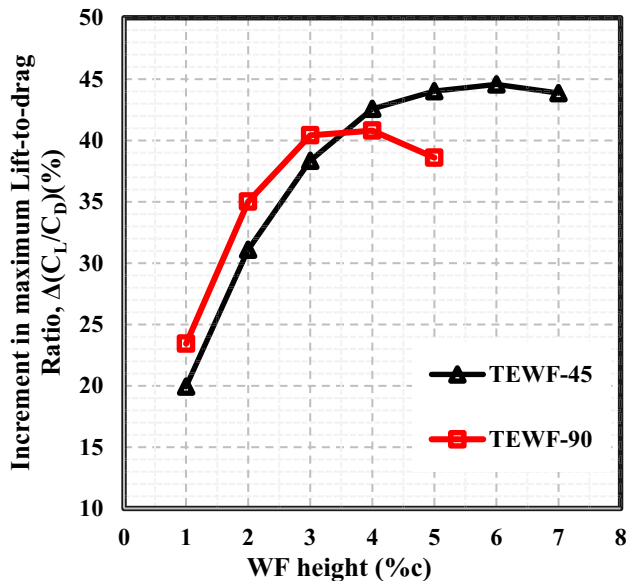


**Fig. 8** Effect of WF height and mounting angle on the aerodynamic characteristics of the NACA0021 airfoil. At the lift side with TEWF-90. **a** Lift. **b** Drag. **c** Lift-to-drag ratio. At the right side with TEWF-45. **d** Lift. **e** Drag. **f** Lift-to-drag ratio



**Table 5** Increments of the maximum value of lift coefficient for different TEWF-90 and TEWF-45 heights in comparison with the clean airfoil case

Airfoil with WF height	Increments in maximum $C_L$ (%)		AOA at Maximum $C_L$	
	TEWF-90	TEWF-45	TEWF-90	TEWF-45
Clean airfoil	–	–	14	14
with 1% WF	25.09	19.19	13	13
with 2% WF	38.39	32.05	13	13
with 3% WF	50.94	41.69	12	12
with 4% WF	61.83	50.21	12	12
with 5% WF	70.19	57.13	11	12
with 6% WF	–	63.69	–	12
with 7% WF	–	69.15	–	11

**Fig. 9** Increments in the values of maximum lift-to-drag ratio at different WF heights and angles compared with the clean airfoil

presented in Table 6, Figs. 10 and 11. In previous sections, the investigations were performed to find the optimum WF height and angle attached to the symmetrical airfoil NACA0021 at  $L/H=1$ . In the present section, the effect of different WF lengths at an optimum fixed height (resulting from the last section) and different mounting angles on the performance of static NACA0021 will be performed. Different  $L/H$  ratios have been studied  $L/H < 1$  and  $L/H > 1$ . The  $C_L$ -AOA curves show positive increments of maximum lift at  $L/H < 1$  for TEWF-90 and TEWF-45 cases, while at  $L/H > 1$ , the increment of maximum  $C_L$  values becomes

negative be due to the penalty of drag due to extending the length upstream.

The lift coefficient curve shows a higher lift value for the TEWF-90 case at  $L/H=0.125$  ratio with a higher penalty of drag resulting in the low values of lift-to-drag ratio as shown in Figs. 10c and 11, and this might be happened due to the vortex tip losses occurs with thin WF. As the  $L/H$  ratio increases at the pressure side of the airfoil, the lift decreases, and the drag also decreases. Still, the lift-to-drag ratio increased, reaching the maximum value at  $L=H$  before falling again at  $L/H > 1.25$ . Therefore, the optimum lift-to-drag ratio for the TEWF-90 case was achieved at  $L=H$ .

The lift-to-drag ratio curves for TEWF-45 Figs. 10f and 11 show higher increment at low  $L/H$  ratio with a slight degradation of maximum lift-to-drag ratio at thin WF when  $L/H=0.0834$  ( $L=0.5\%$ c). The increments in lift-to-drag ratio have a maximum value of 0.847% at  $L/H=0.0167$ , where the length is 1%c, and the height is 6%c compared with TEWF-45 case at  $L=H=6\%$ c, the increments in maximum lift-to-drag ratio decrease slightly at  $L/H < 0.5$  then, the decrement rate at  $L/H > 1$  increased. Generally, the WFs with  $L/H < 1$  show a slight increment in the aerodynamic performance compared with the higher decrement at  $L/H > 1$ .

### 3.4 Optimum Aerodynamic Characteristics for TEWF-90 and TEWF-45

Comparison of different maximum aerodynamic characteristics for TEWF-90 with 4%c height at  $L=H$ , TEWF-45 with 6%c height at  $L=H$ , and with 6%c height and 1%c length with comparison to clean airfoil case are shown in Fig. 12. As Fig. 12a presents, TEWF-45 with 6%c height and 1%c length shows a higher lift coefficient at  $AOA < 15^\circ$  with a maximum lift force coefficient value of 1.59 at  $AOA=11$  with total increments value of about 71.67% in comparison to clean airfoil case, before its early stall in comparison to TEWF-90 with 4%c. The maximum lift for studied cases shifted the lift by  $2^\circ$  compared to the clean case. Figure 12b shows a reduction in drag of TEWF-45 cases at  $AOA < 10^\circ$  before their increase at higher AOA compared to TEWF-90. The aerodynamic efficiency for TEWF-45 with  $L/H=0.167$  ( $L=1\%$ c) in Fig. 12c shows the highest values of lift-to-drag ratio at low to the medium of AOA range with a maximum increment of 45.79% at  $AOA=6$  compared to the clean airfoil case.

### 3.5 Wedge Flap Versus Gurney Flap

The length and height of WF can control the drag and lift coefficients, respectively, while the GF effectiveness depends on just height, which gives WF more advantages over GF. A



**Table 6** Increment in the values of the maximum lift-to-drag ratio at fixed WF height and with different WF lengths for TEWF-90 at 4%*c* (5.6 mm) and TEWF-45 at 6%*c* (8.4 mm) in comparison with the  $L/H=1$  case

TEWF-90 at $H=4\%c$					TEWF-45 at $H=6\%c$				
WF based on chord length (%)	WF length $L$ (mm)	$L/H$ ratio	Increments in maximum $C_L$ (%)	Increment in maximum Lift-to-drag Ratio, $C_L/C_D$ (%)	WF based on chord length (%)	WF length $L$ (mm)	$L/H$ ratio	Increments in maximum $C_L$ (%)	Increment in maximum Lift-to-drag Ratio, $C_L/C_D$ (%)
0.5% <i>c</i>	0.7	0.125	2.34	- 1.12	0.5% <i>c</i>	0.7	0.0834	<b>5.18</b>	0.831
1% <i>c</i>	1.4	0.25	0.71	- 0.54	1% <i>c</i>	1.4	0.167	4.88	<b>0.847</b>
2% <i>c</i>	2.8	0.5	0.69	- 0.18	2% <i>c</i>	2.8	0.334	4.03	0.827
3% <i>c</i>	4.2	0.75	0.20	- 0.03	3% <i>c</i>	4.2	0.5	3.10	0.737
4% <i>c</i>	5.6	1	0.0	0.0	4% <i>c</i>	5.6	0.67	2.13	0.570
5% <i>c</i>	7	1.25	- 1.21	- 0.04	5% <i>c</i>	7	0.834	1.07	0.324
6% <i>c</i>	8.4	1.5	- 2.48	- 0.17	6% <i>c</i>	8.4	1	0.00	0.0
8% <i>c</i>	11.2	2	- 4.65	- 0.67	7% <i>c</i>	9.8	1.167	- 0.98	- 0.357
12% <i>c</i>	16.8	3	- 8.58	- 2.29	8% <i>c</i>	11.2	1.34	- 1.95	- 0.766
-	-	-	-	-	9% <i>c</i>	12.6	1.5	- 2.91	- 1.193
-	-	-	-	-	18% <i>c</i>	25.2	3	- 9.77	- 5.460

comparison of the lift-to-drag ratio of NACA0021 employed with TEWF-45 with 6%*c* height and length of 1%*c* versus the same airfoil section and chord length equipped with GF with 2.5%*c* height from literature work by Balduzzi et al. (2021) presents in Fig. 13. At AOAs < 5, the performance of TEWF is higher than GFs, which could give the better self-starting capability to WFs over GFs, while at AOAs > 5, the GF could give higher performance before stalling at the same angle. It can also be concluded that GF with 2.5%*c* height can produce nearly the same effect as WF with 6%*c* height. The greater height of WF provides higher stability and mechanical stiffness of the blades (Bechert et al. 2000).

### 3.6 Flow Control Visualizations

The effect of WF control on the flow structure could be understood through flow visualization. Figure 14 shows velocity and pressure distributions and streamlines of NACA0021 airfoil equipped to TEWF-90 with  $h=4\%c$  and TEWF-45 with  $h=6\%c$  compared with flow visualization of the clean airfoil at different AOAs. At AOA = 0°, separation bubbles can be observed at the upstream zone, while two counter-rotating vortices are presented at the downstream zone of the WFs, and the wake streamlines are deflected downward as compared to the clean airfoil case. The TEWF-90 shows higher circulation in the upstream zone than TEWF-45; this might be attributed to the higher lift and drag produced by TEWF-90, while TEWF-45 shows smooth flow deflection, leading to less lift but considerably less drag with enhancing lift-to-drag ratio over TEWF-90.

With increasing AOA, the first appearance of separation point at AOA = 1° for clean airfoil case starting from TE, as shown in Figs. 14 and 15, while TEWF-45 suppressed the separation points till AOA = 5°. At AOA = 7°, the separation point moves slightly forward, and the size of the vortices increases, which leads to more deflection of the flow at the TE, hence increasing the effective downwash. Therefore, the vortices in the wake region are mainly responsible for the pressure difference between suction and pressure surfaces, hence the lift enhancements. The counter-rotating pairs move up at AOA = 12°, where the lift is at its maximum value, and the separation point moves toward the leading edge. At  $x/c \approx 40\%c$  from TE, the locations of the separation points are close for the clean airfoil case and TEWF-45 case, as shown in Fig. 15. Thus, WF can increase the lift by delaying the flow separation in the TE of the airfoil.

A sudden decrease in the lift indicates the occurrence of a dynamic stall with a large turbulent wake behind the TE, as shown in Fig. 14. The stall occurs at AOA 16° and 17° for TEWF-45 and TEWF-90, respectively, compared with the clean airfoil where the stall occurs at AOA = 19°. With more increasing AOA, the airfoil experiences complete flow separation.

At AOA = 0° as shown in Fig. 14, the velocity and pressure contours for clean airfoil show that the stagnation point located precisely at the leading edge of an airfoil and the airflow accelerate to go on either side symmetrically. While at the same AOA in presence of WFs the stagnation point shifted a bit toward pressure side. For AOA = 7° the stagnation point of clean airfoil shifted a bit downstream of the

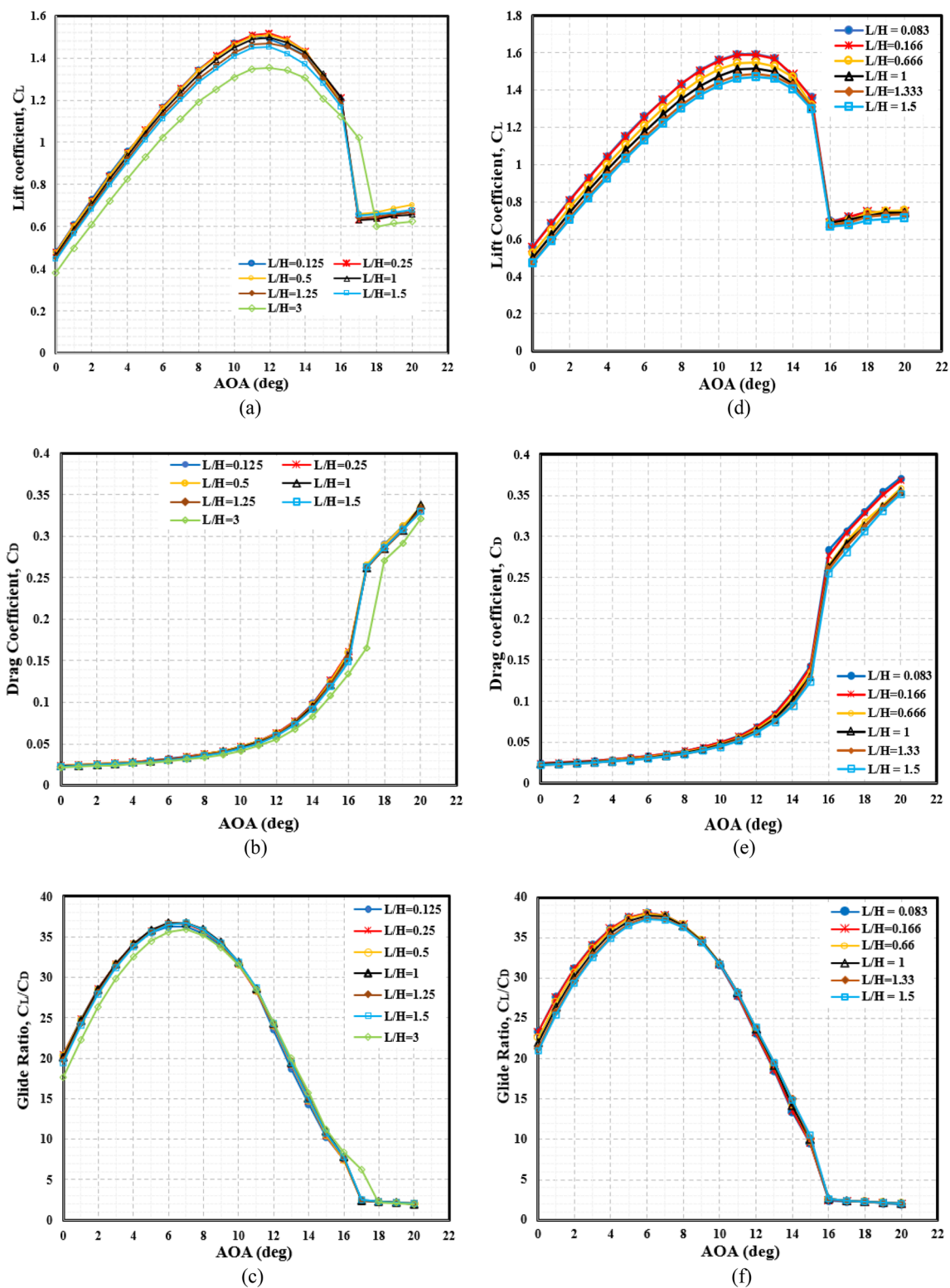
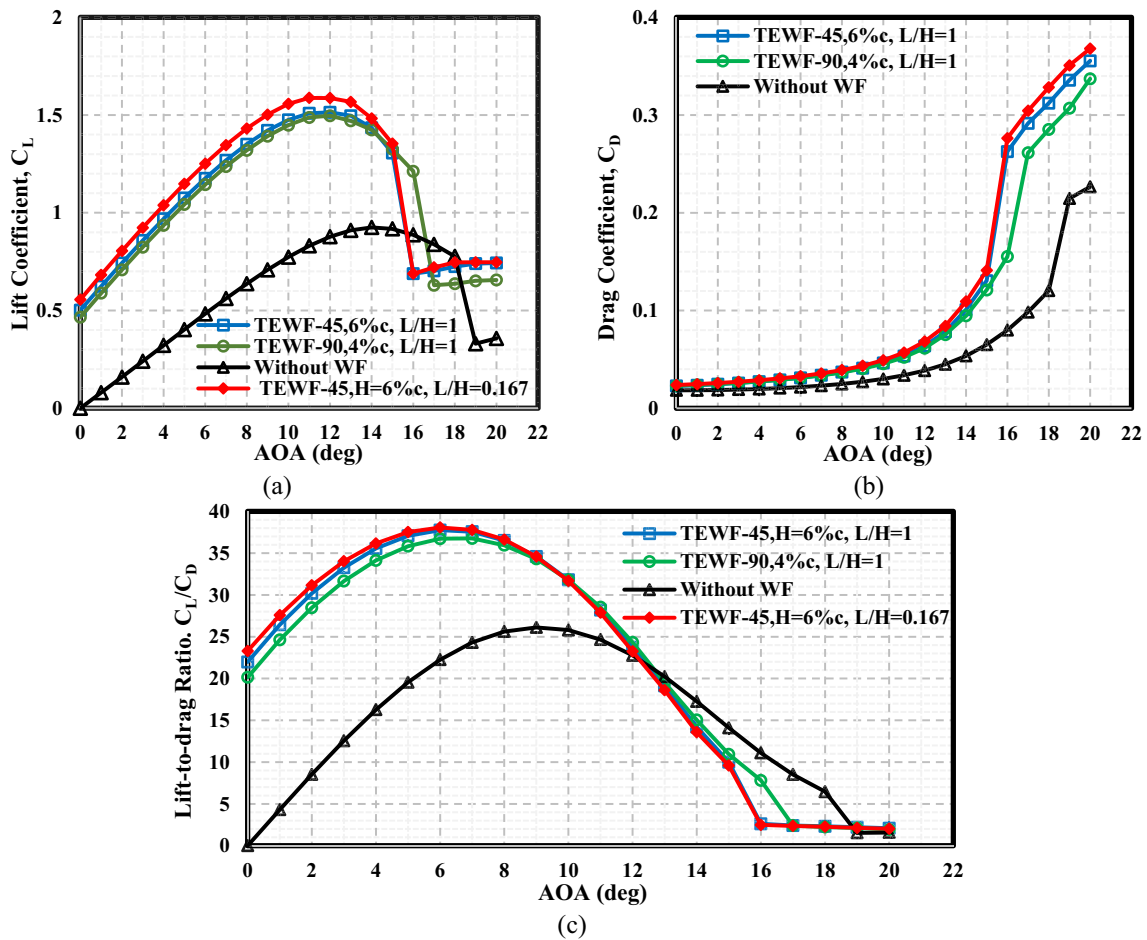
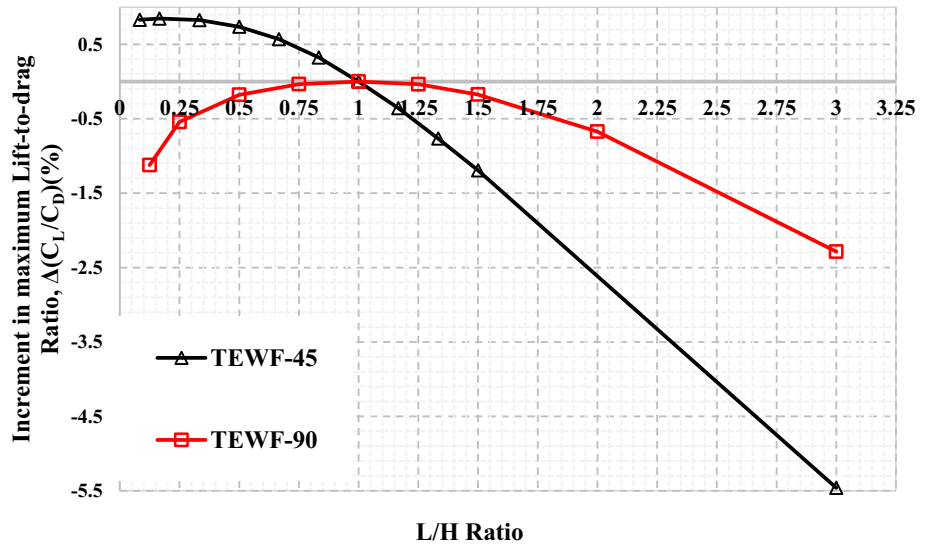


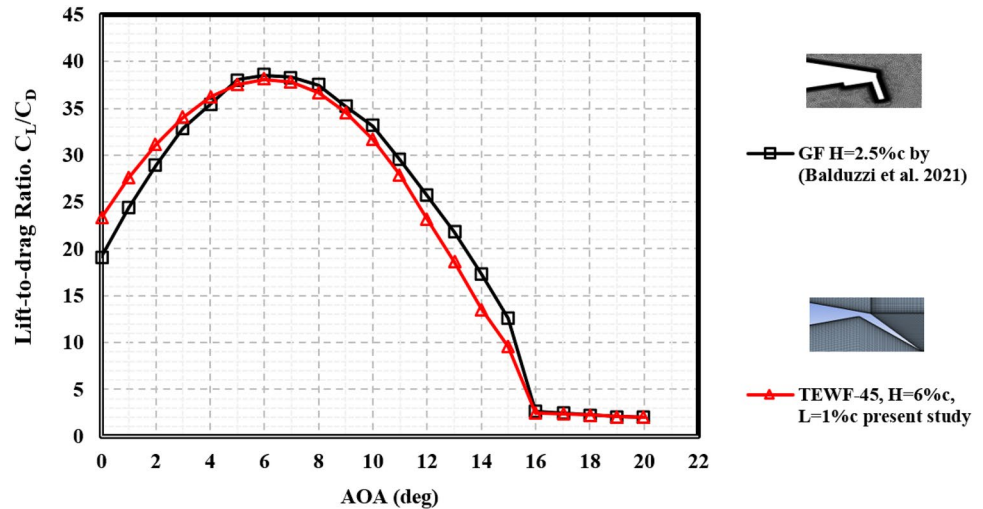
Fig. 10 Effect of WF length and mounting angle on the aerodynamic characteristics of the NACA0021 airfoil. At the lift side with TEWF-90. a Lift. b Drag. c Lift-to-drag ratio. At the right side with TEWF-45. d Lift. e Drag. f Lift-to-drag ratio

**Fig. 11** Increment in the values of maximum lift-to-drag ratio at different WF lengths and angles compared with the  $L/H=1$  case



**Fig. 12** Optimum aerodynamic characteristics for TEWF-90 and TEWF-45 cases in comparison with the clean NACA0021 airfoil case. **a** Lift. **b** Drag. **c** Aerodynamic efficiency

**Fig. 13** Comparing maximum lift-to-drag ratio TEWF-45,  $H=6\%c$ ,  $L=1\%c$  and GF  $H=2.5\%c$  from literature



leading edge. While this shifting toward pressure side clearly observed in presence of WFs at  $AOA = 7^\circ$ .

## 4 Conclusions

In this study, the potential of using WF as a passive flow control device equipped to the wind turbine airfoils (NACA0021) has been studied computationally using ANSYS FLUENT to explore its impact on the flow behavior and aerodynamic performance. Various cases are considered to investigate WF height's effect and  $(L/H)$  variations at angles  $90^\circ$  and  $45^\circ$ . Results showed that deploying WFs changes the Kutta condition and creates a recirculation suction region near the TE's pressure side surface. This suction region enhances the flow pattern on the airfoil; thus, the effective camber line changed, and the pressure distribution between TE upper stream and downstream was affected.

The CFD model from this study could adequately capture the aerodynamic characteristics and the flows over the modified airfoil. To conclude, the main findings are as follows:

- The optimum WF height at a  $90^\circ$  mounting angle is  $4\%c$  with a maximum increment in the lift-to-drag ratio of  $40.80\%$  at  $AOA = 7^\circ$  compared to the clean airfoil.
- The optimum WF height at a  $45^\circ$  mounting angle is  $6\%c$  with a maximum increment in lift-to-drag ratio of  $44.57\%$  at  $AOA = 6^\circ$  compared with the clean airfoil.
- Thin WFs with  $L < 1\%c$  show the highest lift coefficient but with slight degradation of the maximum glide ratio, which may be attributed to the vortex tip losses at blade tips.

- The maximum increment value in lift-to-drag ratio due to variations of  $L/H$  is  $0.847\%$  at  $L/H = 0.0167$ ,  $L = 1\%c$  and the  $H = 6\%c$  compared to TEWF-45 case at  $L = H = 6\%c$ ,
- The WFs with  $L/H < 1$  show a slight increment in the aerodynamic performance, while at  $L/H > 1$  indicate a higher performance decrease compared with the  $L/H = 1$  case.
- The TEWF-45 with  $H = 6\%c$  and  $L = 1\%c$  suppressed the separation points till  $AOA = 5^\circ$  and achieved maximum  $C_L$  and  $C_L/C_D$  values at  $AOA = 11^\circ$  and  $6^\circ$  with total increment values of about  $71.67\%$  and  $45.79\%$ , respectively, in comparison with the clean airfoil case.
- Trailing edge WF shows higher performance than GF for the same airfoil section and Re number at  $AOA < 5$ , which might give better self-starting capability to WFs than GFs.
- It can also be concluded that Gf with  $2.5\%c$  height can produce nearly the same effect as WF with  $6\%c$  height. The greater height of WF provides higher stability and mechanical stiffness of the blade.
- The presence of WFs at certain AOA's adds a further effect of shifting the leading-edge stagnation point on the airfoil toward the pressure side of the airfoil, which is associated with increased circulation, resulting in lift enhancement.
- The vortices acting on the downstream face of the WF are mainly responsible for the pressure difference between suction and pressure surfaces, hence the lift enhancements.

As a passive flow control device, WF can potentially suppress the separation point and enhance aerodynamic



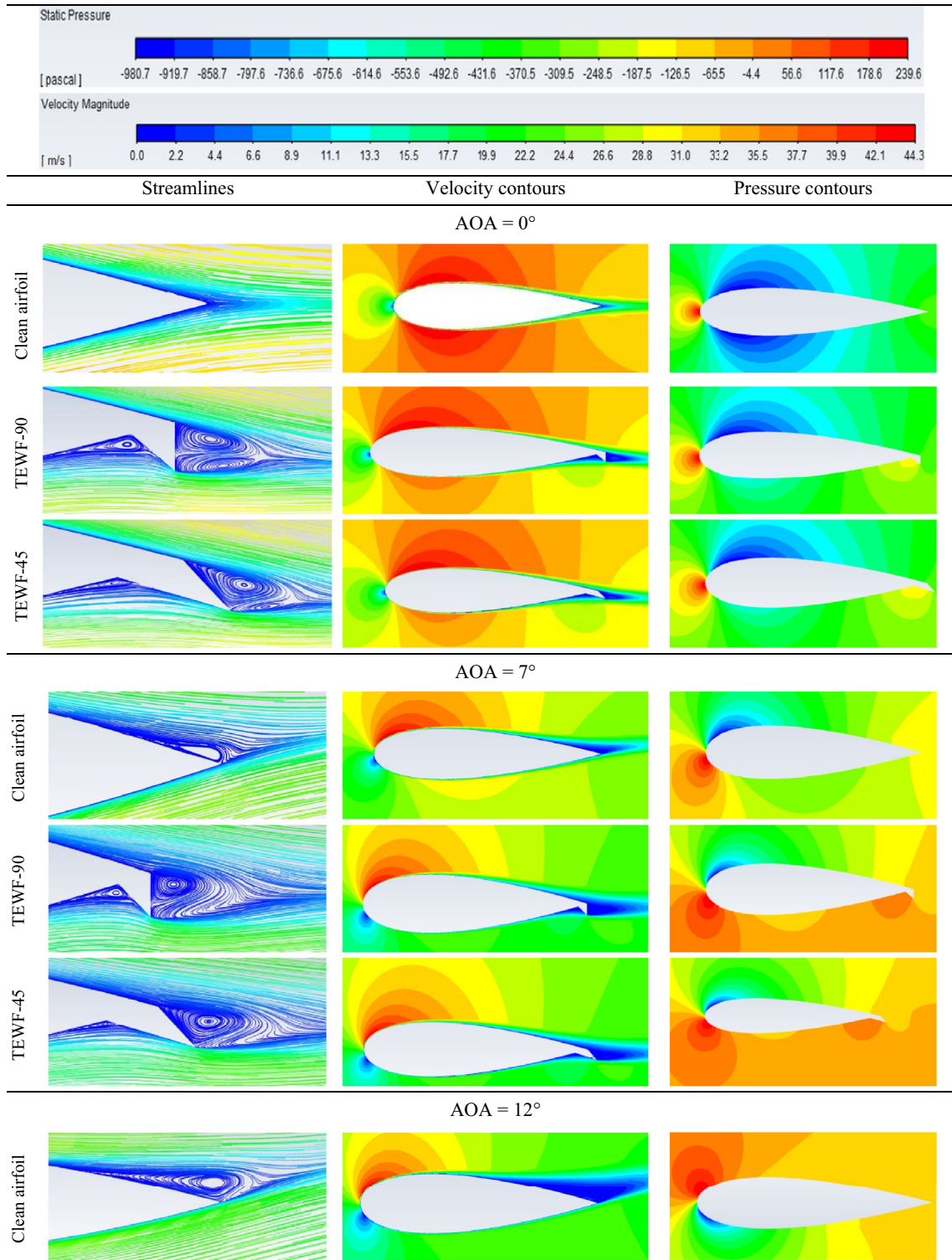


**Fig. 14** Streamlines, pressure, and velocity distributions for TEWF-90 and TEWF-45 at different AOAs in comparison with clean NACA0021 airfoil



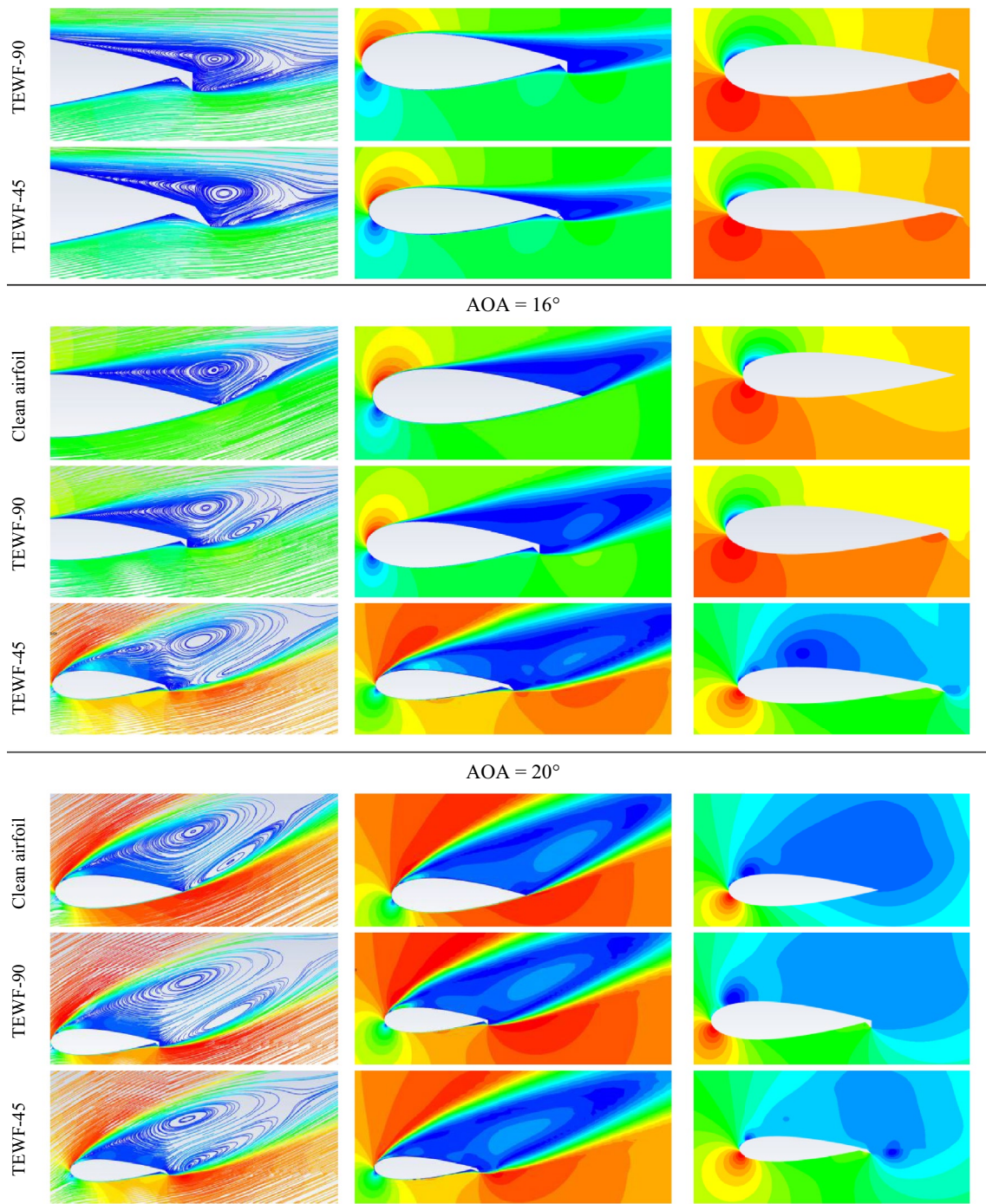
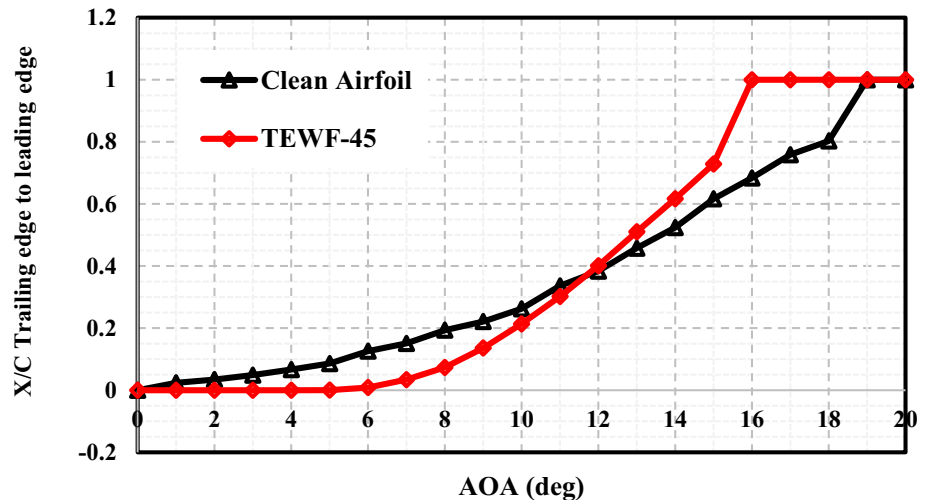


Fig. 14 (continued)

performance. The findings of the current study help to better understand the influence of airfoils employed with WF on the aerodynamic performance of different applications, such as aeronautics and rotating rotor blades. However, the investigations were limited to  $Re = 180k$  on a symmetric airfoil section in 2D. Further studies could be done to

explore the effects of different  $Re$  numbers and asymmetric airfoil sections in 3D. Moreover, the developments could consider using WFs at optimal configurations in vertical axis wind turbine design or in combination with different passive flow control techniques.

**Fig. 15** Separation point development versus AOA along airfoil chord length for TEWF-45 compared with clean NACA0021 airfoil



**Acknowledgements** The research is funded by the Universiti Kebangsaan Malaysia under the Research University Grant (GUP-2023-064).

**Data Availability** Some or all data, models, or codes that support the findings of this study are available from the corresponding author upon reasonable request.

## References

- Akhlagi M, Ghafoorian F, Mehrpooya M, Sharifi Rizzi M (2023) Effective parameters optimization of a small scale gorlov wind turbine, using CFD method. *Iran J Chem Chem Eng* 42(7):2311–2329. <https://doi.org/10.30492/ijcce.2022.561960.5584>
- Anderson D, Tannehill JC, Pletcher RH (2016) Computational fluid mechanics and heat transfer. 3rd edn
- Asadbeigi M, Ghafoorian F, Mehrpooya M, Chegini S, Jarrahan A (2023) A 3D study of the darrieus wind turbine with auxiliary blades and economic analysis based on an optimal design from a parametric investigation. *Sustainability*. <https://doi.org/10.3390/su15054684>
- Azlan F, Tan MK, Tan BT, Ismadi MZ (2023) Passive flow-field control using dimples for performance enhancement of horizontal axis wind turbine. *Energy*. <https://doi.org/10.1016/j.energy.2023.127090>
- Balduzzi F, Holst D, Melani PF, Wegner F, Nayeri CN, Ferrara G, Paschereit CO, Bianchini A (2021) Combined numerical and experimental study on the use of gurney flaps for the performance enhancement of NACA0021 airfoil in static and dynamic conditions. *J Eng Gas Turbines Power* 143(2):4. <https://doi.org/10.1115/1.4048908>
- Bangga G, Hutani S, Heramarwan H (2021) The effects of airfoil thickness on dynamic stall characteristics of high-solidity vertical axis wind turbines. *Adv Theory Simul*. <https://doi.org/10.1002/adts.202000204>
- Bechert DW, Meyer R, Hage W (2000) Drag reduction of airfoils with miniflaps. Can we learn from dragonflies? In: *Fluids 2000 conference and exhibit*. <https://doi.org/10.2514/6.2000-2315>
- Belamadi R, Settari A, Chetehouna K, Ilinca A (2022) Numerical modeling of horizontal axis wind turbine: aerodynamic performances improvement using an efficient passive flow control system. *Energies*. <https://doi.org/10.3390/en15134872>
- Bloy AW, Tsioumanis N, Mellor NT (1997) Enhanced aerofoil performance using small trailing-edge flaps. *J Aircr*. <https://doi.org/10.2514/2.2210>
- Boyd JA (1985) Trailing edge device for an airfoil. United States Patent, Patent Number: 4,542,868, 1–6
- Daróczy L, Janiga G, Petrasch K, Webner M, Thévenin D (2015) Comparative analysis of turbulence models for the aerodynamic simulation of H-Darrieus rotors. *Energy* 90:680–690
- Du L, Ingram G, Dominy RG (2019) Experimental study of the effects of turbine solidity, blade profile, pitch angle, surface roughness, and aspect ratio on the H-Darrieus wind turbine self-starting and overall performance. *Energy Sci Eng*. <https://doi.org/10.1002/ese3.430>
- Farajyar S, Ghafoorian F, Mehrpooya M, Asadbeigi M (2023) CFD investigation and optimization on the aerodynamic performance of a savonius vertical axis wind turbine and its installation in a hybrid power supply system: a case study in Iran. *Sustainability*. <https://doi.org/10.3390/su15065318>
- Florin F, Horia D, Alexandru D (2014) Numerical investigations of dynamic stall control. *INCAS Bull* 6(Special 1):67–80. <https://doi.org/10.13111/2066-8201.2014.6.S1.8>
- Ghazali MI, Harun Z, WanGhopa WA, Abbas AA (2016) Computational fluid dynamic simulation on NACA 0026 airfoil with V-groove riblets. *Int J Adv Sci Eng Inf Technol*. <https://doi.org/10.18517/ijaseit.6.4.901>
- Giguère P, Dumas G, Lemay J (1997) Gurney flap scaling for optimum lift-to-drag ratio. *AIAA J*. <https://doi.org/10.2514/2.49>
- Hand B, Kelly G, Cashman A (2017) Numerical simulation of a vertical axis wind turbine airfoil experiencing dynamic stall at high Reynolds numbers. *Comput Fluids*. <https://doi.org/10.1016/j.compfluid.2017.02.021>
- Holst D, Balduzzi F, Bianchini A, Church B, Wegner F, Pechlivanoglou G, Ferrari L, Ferrara G, Nayeri CN, Paschereit CO (2019a) Static and dynamic analysis of a NACA 0021 airfoil section at low Reynolds numbers based on experiments and computational fluid dynamics. *J Eng Gas Turbines Power*. <https://doi.org/10.1115/1.4041150>
- Holst D, Church B, Pechlivanoglou G, Tüzüner E, Saverin J, Nayeri CN, Paschereit CO (2019b) Experimental analysis of a NACA 0021 airfoil section through 180-degree angle of attack at low Reynolds numbers for use in wind turbine analysis. *J Eng Gas Turbines Power*. <https://doi.org/10.1115/1.4041651>

- Holst D, Church B, Wegner F, Pechlivanoglou G, Nayeri CN, Paschereit CO (2019c) Experimental analysis of a NACA 0021 airfoil under dynamic angle of attack variation and low Reynolds numbers. *J Eng Gas Turbines Power*. <https://doi.org/10.1115/1.4041146>
- Jha SK, Gautam U, Pawar P, Narayanan S, Kumaraswamidhas LA (2020) Investigations of flow phenomena over a flat plate and NACA0012 airfoil at high angles of attack. *Iran J Sci Technol Trans Mech Eng*. <https://doi.org/10.1007/s40997-019-00313-z>
- Lee T (2009) Aerodynamic characteristics of airfoil with perforated Gurney-type flaps. *J Aircr*. <https://doi.org/10.2514/1.38474>
- Li Y, Wang J, Zhang P (2002) Effects of Gurney flaps on a NACA0012 airfoil. *Flow Turbul Combust*. <https://doi.org/10.1023/A:1015679408150>
- Li Q, Maeda T, Kamada Y, Hiromori Y, Nakai A, Kasuya T (2017) Study on stall behavior of a straight-bladed vertical axis wind turbine with numerical and experimental investigations. *J Wind Eng Ind Aerodyn*. <https://doi.org/10.1016/j.jweia.2017.02.005>
- Liebeck RH (1978) Design of subsonic airfoils for high lift. *J Aircr*. <https://doi.org/10.2514/3.58406>
- Meyer R, Hage W, Bechert DW, Schatz M, Thiele F (2006) Drag reduction on gurney flaps by three-dimensional modifications. *J Aircr*. <https://doi.org/10.2514/1.14294>
- Michna J, Rogowski K, Bangga G, Hansen MOL (2021) Accuracy of the gamma re-theta transition model for simulating the DU-91-W2-250 airfoil at high Reynolds numbers. *Energies*. <https://doi.org/10.3390/en14248224>
- Mohamed MH (2012) Performance investigation of H-rotor Darrieus turbine with new airfoil shapes. *Energy* 47(1):522–530. <https://doi.org/10.1016/j.energy.2012.08.044>
- Mohammadi M, Doosttalab A, Doosttalab M (2012) The effect of various gurney flap shapes on the performance of wind turbine airfoils. In: ASME early career technical conference, 11 November (2012)
- Myose R, Heron I, Papadakis M (1996) The post-stall effect of Gurney flaps on a NACA-0011 airfoil. *SAE Techn Pap*. <https://doi.org/10.4271/961316>
- Neuhart DH, Pendergraft IC (1988) Water tunnel study of Gurney Flaps. In: NASA technical memorandum (Issue 4071).
- Ni L, Miao W, Li C, Liu Q (2021) Impacts of Gurney flap and solidity on the aerodynamic performance of vertical axis wind turbines in array configurations. *Energy*. <https://doi.org/10.1016/j.energy.2020.118915>
- Özkan M, Erkan O (2022) Control of a boundary layer over a wind turbine blade using distributed passive roughness. *Renew Energy*. <https://doi.org/10.1016/j.renene.2021.11.082>
- Paraschivoiu I (2002) *Wind turbine design: with emphasis on Darrieus concept*. Presses inter Polytechnique
- Ramlee MF, Fazlizan A, Mat S (2020) Performance evaluation of H-type Darrieus vertical axis wind turbine with different turbine solidity. *J Comput Theor Nanosci* 17(2–3):833–839
- Rezaeiha A, Montazeri H, Blocken B (2018a) Characterization of aerodynamic performance of vertical axis wind turbines: impact of operational parameters. *Energy Convers Manag*. <https://doi.org/10.1016/j.enconman.2018.05.042>
- Rezaeiha A, Montazeri H, Blocken B (2018b) Toward optimal aerodynamic design of vertical axis wind turbines: impact of solidity and number of blades. *Energy* 165:1129–1148. <https://doi.org/10.1016/j.energy.2018.09.192>
- Rezaeiha A, Montazeri H, Blocken B (2019) On the accuracy of turbulence models for CFD simulations of vertical axis wind turbines. *Energy* 180:838–857. <https://doi.org/10.1016/j.energy.2019.05.053>
- Richter K, Rosemann H (2002) Experimental investigation of trailing-edge devices at transonic speeds. *Aeronaut J* 106(1058):185
- Storms BL, Jang CS (1994) Lift enhancement of an airfoil using a Gurney flap and vortex generators. *J Aircr*. <https://doi.org/10.2514/3.46528>
- Timmer WA, Van Rooij RPJOM (2003) Summary of the Delft University wind turbine dedicated airfoils. *J Sol Energy Eng Trans ASME*. <https://doi.org/10.1115/1.1626129>
- Troolin DR, Longmire EK, Lai WT (2006) Time resolved PIV analysis of flow over a NACA 0015 airfoil with Gurney flap. *Exp Fluids*. <https://doi.org/10.1007/s00348-006-0143-8>
- Wang H, Zhang B, Qiu Q, Xu X (2017) Flow control on the NREL S809 wind turbine airfoil using vortex generators. *Energy*. <https://doi.org/10.1016/j.energy.2016.11.003>
- Wang S, Ingham DB, Ma L, Pourkashanian M, Tao Z (2010) Numerical investigations on dynamic stall of low Reynolds number flow around oscillating airfoils. *Comput Fluids* 39(9):1529–1541
- White F, Xue H (2021) *Fluid mechanics*, 9th edn. McGraw-Hill Education, New York
- Yan Y, Avital E, Williams J, Cui J (2020) Performance improvements for a vertical axis wind turbine by means of gurney flap. *J Fluids Eng Trans ASME*. <https://doi.org/10.1115/1.4044995>
- Zhong J, Li J, Guo P, Wang Y (2019) Dynamic stall control on a vertical axis wind turbine aerofoil using leading-edge rod. *Energy*. <https://doi.org/10.1016/j.energy.2019.02.176>
- Zhu H, Hao W, Li C, Ding Q, Wu B (2018) A critical study on passive flow control techniques for straight-bladed vertical axis wind turbine. *Energy*. <https://doi.org/10.1016/j.energy.2018.09.072>

Springer Nature or its licensor (e.g. a society or other partner) holds exclusive rights to this article under a publishing agreement with the author(s) or other rightsholder(s); author self-archiving of the accepted manuscript version of this article is solely governed by the terms of such publishing agreement and applicable law.